Sādhanā (2022)47:219
https://doi.org/10.1007/s12046-022-01951-x

Analytical solution of thermally developing heat transfer in circular and parallel plates microchannels

LIANGBIN SU[1,2,3], BOSHU HE[3] and WAN YU[1,2,*]

[1]Hubei Key Laboratory of Hydroelectric Machinery Design and Maintenance, China Three Gorges University, Yichang 443002, China
[2]College of Mechanical and Power Engineering, China Three Gorges University, Yichang 443002, China
[3]Institute of Combustion and Thermal Systems, School of Mechanical, Electronic and Control Engineering, Beijing Jiaotong University, Beijing 100044, China
e-mail: yuwan@ctgu.edu.cn

MS received 16 January 2022; revised 6 May 2022; accepted 21 June 2022

Abstract. The heat transfer characteristics of the thermally developing flow in the circular and parallel plates microchannels under the constant wall temperature and the constant heat flux are studied analytically. The energy equations are solved by using the separation of variables combined with the Gram–Schmidt orthogonalization. The effect of the number of eigenvalues on the calculation accuracy of the local Nusselt number is first determined. The temperature distribution and the heat transfer coefficient at the entrance region are calculated considering the effects of the rarefaction ($0 < Kn < 0.1$) and the axial heat conduction ($Pe > 50$). It is found that the axial heat conduction can dramatically improve the heat transfer of the thermally developing flow when the Peclet number is less than 250. But when the Peclet number is greater than 500, the effect of the axial heat conduction can be omitted. Enhancing the rarefaction would weaken the influence of the axial heat conduction on the heat transfer, and the difference of the local Nusselt number between the two boundary conditions decreases as increasing *Kn*. Enhancing fluid axial heat conduction would increase the thermal entrance length. The thermal entrance length of the microtube is 3–4 times that of the parallel plates microchannel, and the correlations of the thermal entrance lengths are developed, which may provide guidance for thermal design and optimization of microchannel heat sinks.

Keywords. Entrance effect; rarefaction effect; axial heat conduction; constant wall temperature; constant heat flux.

1. Introduction

With the development of the modern micro-electro-mechanical system and the continuous improvement of packaging density, the heat dissipation requirements of nanoscale chips in conventional microelectronic devices have reached 10 MW/m^2. Such a large amount of heat dissipation puts forward higher requirements on the thermal management system. It is necessary to configure the best cooling system to ensure the device operates properly and prolong the cycle life of the device. While conventional heat exchangers are cumbersome and cannot handle such high heat flux density. The microchannel heat exchanger emerges as the engineering requires. The tiny size is a distinguishing feature of microchannels. The Knudsen number *Kn*, defined as the ratio of the mean free path λ to the length scale characteristic D_h [1], increases as the characteristic length decreases. As $0.001<Kn<0.1$, the well-known Navier–Stokes equations are still appropriate for the fluid, but velocity slip and temperature jump boundary conditions are required to modify the fluid-solid interface.

When the channel is short in mini-structured devices, the entrance effect has to be taken into account. The heat transfer capacity of the thermally developing flow in a channel is significantly higher than that of the fully developed region because of the entrance effect. The convective heat transfer problem of the thermally developing flow in a channel is also named Graetz problem [2]. Shah and London [3] summarized plentiful results about the Graetz problem in various macro channels. In 1997, Barron *et al* [4] first extended the problem to include the effects of slip flow through the microtube (CM) with the constant wall temperature by using the Frobenius series method [5]. They found the Nusselt number increases as the Knudsen number, meaning that the rarefaction effect in the microchannel enhances the heat transfer, which is different from other results [6–9]. Larrode *et al* [7] and Tunc and

*For correspondence
Published online: 29 October 2022

Bayazitoglu [8] pointed out that the rarefaction effect weakens the heat transfer performance, and the results in Barron *et al* [4] are due to ignoring the temperature jump boundary condition during the calculation. Therefore, the flow and heat transfer characteristics in the microchannel still meet the Reynolds analogy [10, 11].

The velocity profile is fully developed for the Graetz problem. The problem of the thermally developing flow can be thus solved with some theoretical methods. Apart from the aforementioned series method, some other methods are also applied to study the Graetz problem. Chalhub *et al* [12] obtained the solution of the extended Graetz problem in isothermal parallel plates microchannels (PPM) based on the Generalized Integral Transform Technique. They considered the effects of the axial conduction and the rarefaction on the local Nusselt number and found the influence of the axial conduction declined as increasing the rarefaction. Haddout *et al* [13] also studied a similar problem in both CM and PPM. They degraded the energy equation into two first-order partial differential equations by using the self-adjoint formalism and indicated that the local Nusselt number was strongly influenced by the Peclet and Knudsen numbers. What's more, the separation of variables was often employed to settle the extended Graetz problem [14, 15].

Nevertheless, it is worth noting that the influence of the axial fluid heat conduction, characterized by the Peclet number *Pe*, on the heat transfer performance of the thermally developing flow in microchannels was often ignored in most of the above analytical results. Many studies about the thermally developing flow were also based on the assumption of ignoring the axial heat conduction [16–24]. While the axial heat conduction even dominates the heat transfer process when the Peclet number is low enough [25–28]. However, it is not clear when the axial heat conduction should be considered. Tada and Ichimiya [29] pointed out that the effect of the axial heat conduction can be neglected when $Pe>200$. But Renksizbulut and Niazmand [30] demonstrated that the local Nusselt number was independent of *Pe* when $Pe>50$. Avci and Aydin [31] found that the axial heat conduction had little effect on heat transfer when $Pe>5$. While some investigations showed that the influence of the axial heat conduction on the convective heat transfer was obvious when $Pe<100$ [32–43]. The inconsistent results indicate that the importance of the axial heat conduction on heat transfer of the developing flow remains to be further determined.

The objective of this work is to determine the impacts of the axial heat conduction ($Pe>50$) and rarefaction ($0<Kn<0.1$) on forced convection heat transfer in both CM and PPM. The motivation is to figure out the criteria for ignoring or considering the effect of axial conduction in microchannels. Two types of thermal boundary conditions, namely constant wall temperature and constant heat flux, are taken into consideration. The energy equation is solved by using the separation of variables. The effect of the number of eigenvalues on the calculation accuracy of the local Nusselt number is first investigated. The Gram–Schmidt orthogonalization is utilized to solve the nonorthogonal boundary problems caused by considering the axial heat conduction. The heat transfer performance under different thermal boundary conditions is also compared. The thermal entrance lengths of different microchannels with different boundary conditions are also calculated, which may provide the guideline for the design of microchannel heat sinks.

2. Analysis

The velocity is fully developed for the Graetz problem as illustrated in figure 1 and the flow chart of the analytical solution is shown in figure 2. For laminar flow, the general form of the energy equation is expressed as follows [44]

$$\rho c_p \frac{DT}{Dt} = \nabla \cdot (\kappa \nabla T) + Q + \beta T \frac{DP}{Dt} + \mu \Phi \qquad (1)$$

where Q is internal heat generation, β is the coefficient of thermal expansion, μ is the dynamic viscosity, ρ is the density, c_p is the specific heat, κ is the thermal conductivity and Φ is the viscous dissipation function. The viscous dissipation can be ignored with the huge heat flux and small dynamic viscosity of air in the present work. With the assumption of ignoring the effects of viscous dissipation, natural convection, and radiation heat transfer, the energy equation of constant thermophysical properties and incompressible Newtonian fluid without internal heat generation in parallel plates and circular tubes can be simplified to

$$\rho c_p u \frac{\partial T}{\partial x} = \kappa \left[\frac{1}{r^p} \frac{\partial}{\partial n} \left(r^p \frac{\partial T}{\partial n} \right) + \frac{\partial^2 T}{\partial x^2} \right] \qquad (2)$$

The geometry factor p (or n) is 0 (or y) in PPM and 1 (or r) in CM. Before solving the energy equation, defining the following non-dimensional quantities,

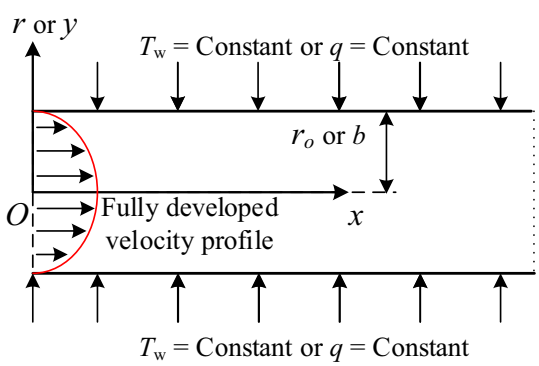

Figure 1. Schematic diagram and coordinate system.

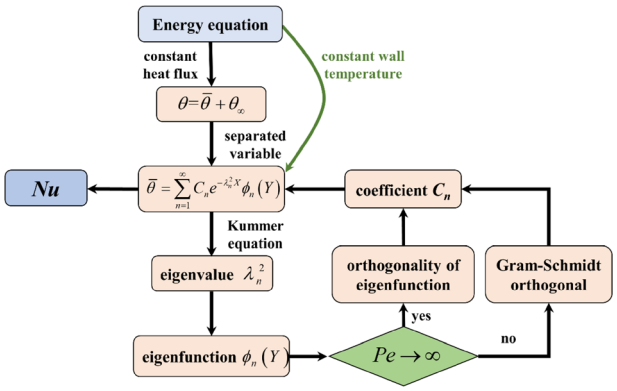

Figure 2. Flow chart of the analytical solution.

$$\text{CM}: \quad A=\sqrt{\frac{1}{1+4Kn_u}},\ X=\frac{A^2(2-A^2)x}{r_o Pe},\ Y=\frac{n}{r_o}A,\ \overline{Pe}=\frac{Pe}{A(2-A^2)}$$
$$\text{PPM}: \quad A=1+12Kn_u,\ B=\frac{1+8Kn_u}{A^2},\ Y=\frac{n}{Ab},\ \overline{Pe}=\frac{3}{8}PeA^2 \tag{3}$$

where Kn_u, defined as $Kn(2–\sigma_v)/\sigma_v$, is the modified Knudsen number [45] and the corresponding tangential momentum accommodation coefficient σ_v is set as unity in this paper. Based on these non-dimensional quantities, Eq. (2) is transformed into

$$\left(B^{1-p}-Y^2\right)\frac{\partial\theta}{\partial X}=\frac{1}{Y^p}\frac{\partial}{\partial Y}\left(Y^p\frac{\partial\theta}{\partial Y}\right)+\frac{1}{\overline{Pe}^2}\frac{\partial^2\theta}{\partial X^2} \tag{4}$$

where θ is the no-dimensional temperature and defined as

$$\theta=\begin{cases}\dfrac{T-T_{\text{in}}}{D_h q/\kappa} & \textit{constant heat flux}\\ \dfrac{T-T_{\text{w}}}{T_{\text{in}}-T_{\text{w}}} & \textit{constant wall temperature}\end{cases} \tag{5}$$

where T_{in} is the inlet temperature of the working medium.

2.1 *Constant heat flux*

The non-dimensional boundary conditions for the constant heat flux are as follows

$$\theta(0,Y)=0 \tag{6}$$
$$\theta(\infty,Y)=\theta_\infty \tag{7}$$
$$\left.\frac{\partial\theta}{\partial Y}\right|_{Y=0}=0 \tag{8}$$
$$\left.\frac{\partial\theta}{\partial Y}\right|_{Y=A^{2p-1}}=1 \tag{9}$$

where θ_∞ is the no-dimensional temperature in the fully developed region. As Eq. (4) is a linear equation, according to the superposition principle, we have

$$\theta=\overline{\theta}+\theta_\infty \tag{10}$$

For the new variable $\overline{\theta}$, the corresponding equation and the boundary conditions are

$$\left(B^{1-p}-Y^2\right)\frac{\partial\overline{\theta}}{\partial X}=\frac{1}{Y^p}\frac{\partial}{\partial Y}\left(Y^p\frac{\partial\overline{\theta}}{\partial Y}\right)+\frac{1}{\overline{Pe}^2}\frac{\partial^2\overline{\theta}}{\partial X^2} \tag{11}$$
$$\overline{\theta}(0,Y)=-\theta_\infty \tag{12}$$
$$\overline{\theta}(\infty,Y)=0 \tag{13}$$
$$\left.\frac{\partial\overline{\theta}}{\partial Y}\right|_{Y=0}=0 \tag{14}$$
$$\left.\frac{\partial\overline{\theta}}{\partial Y}\right|_{Y=A^{2p-1}}=0 \tag{15}$$

Due to the homogeneous boundary conditions in the Y direction, the equation has an infinite series solution of the following form

$$\overline{\theta}=\sum_{n=1}^{\infty}C_n e^{-\lambda_n^2 X}\phi_n(Y) \tag{16}$$

where C_n, λ_n^2, $\phi_n(Y)$ are the coefficients, eigenvalues, and eigenfunctions respectively. Substituting Eq. (16) into Eqs. (11), (14), and (15) yields

$$\frac{1}{Y^p}\frac{\mathrm{d}}{\mathrm{d}Y}\left(Y^p\frac{\mathrm{d}\phi_n}{\mathrm{d}Y}\right)+\left(B^{1-p}-Y^2+\frac{1}{\overline{Pe}^2}\lambda_n^2\right)\lambda_n^2\phi_n=0 \tag{17}$$
$$\left.\frac{\mathrm{d}\phi_n}{\mathrm{d}Y}\right|_{Y=0}=0 \tag{18}$$
$$\left.\frac{\mathrm{d}\phi_n}{\mathrm{d}Y}\right|_{Y=A^{2p-1}}=0 \tag{19}$$

In order to solve Eq. (17), choosing $\eta=\lambda_n Y^2$, $\omega(\eta)=e^{\frac{\eta}{2}}\phi_n(\eta)$ gives

$$\eta\frac{\mathrm{d}^2\omega}{\mathrm{d}\eta^2}+\left(\frac{p+1}{2}-\eta\right)\frac{\mathrm{d}\omega}{\mathrm{d}\eta}+\left(B^{1-p}\lambda_n-p-1+\frac{\lambda_n^3}{Pe^2}\right)\frac{\omega}{4}=0 \tag{20}$$

$$\left(-\frac{\omega}{2}+\frac{\mathrm{d}\omega}{\mathrm{d}\eta}\right)_{\eta=\lambda_n A^{4p-2}}=0 \tag{21}$$

Equation (20) is a confluence hypergeometric equation, also known as the Kummer's equation [46]. The eigenvalues can be obtained by solving Eq. (21) with the characteristic of the Kummer's equation. Equation. (21) is then transformed into

$$\frac{4a}{1+p}F(a+1,c+1,z)=F(a,c,z) \tag{22}$$

where the term $F(a,c,z)$ is the Kummer's confluent hypergeometric function and the related parameters are as follows

$$a=\frac{1+p}{4}-\frac{\lambda_n^3}{4\overline{Pe}^2}-\frac{B^{1-p}\lambda_n}{4} \tag{23}$$

$$c=\frac{1+p}{2} \tag{24}$$

$$z=\lambda_n A^{4p-2} \tag{25}$$

λ_n^2 can be acquired by solving Eq. (22) using the FindRoot command in Mathematica. But when it comes to solving the coefficients C_n, it is necessary to discuss the orthogonality of $\phi_n(Y)$.

For the case $Pe \to \infty$, namely ignoring the influence of the axial heat conduction, $\phi_n(Y)$ are mutually orthogonal and C_n can be calculated as follows

$$C_n=\frac{\int_0^{A^{2p-1}}-\theta_\infty(B^{1-p}-Y^2)\phi_n Y^p \mathrm{d}Y}{N(\phi)} \tag{26}$$

where the normalization integrals $N(\phi)$ is expressed as

$$N(\phi)=\int_0^{A^{2p-1}}\left(B^{1-p}-Y^2\right)\phi_n^2 Y^p \mathrm{d}Y \tag{27}$$

Therefore, for CM,

$$C_{n,\mathrm{c}}=\frac{(2A^2-A^4)\phi(A)}{\lambda_n^2 A^2(A^2-2)N(\phi)} \tag{28}$$

For PPM,

$$C_{n,\mathrm{p}}=\frac{(1-3A^2B)\phi_n(A^{-1})}{2\lambda_n^2 N(\phi)} \tag{29}$$

However, $\phi_n(Y)$ are not mutually orthogonal when considering the axial heat conduction. For this case, the Gram-Schmidt orthogonal procedure is employed to fulfill the orthogonalization process. The steps of the orthogonal procedure are shown in "Appendix A".

After determining C_n, λ_n^2, $\phi_n(Y)$, the temperature distribution and the local Nusselt number are also determined. For CM,

$$Nu(x)_{\mathrm{c}}=\frac{2}{\sum_{n=1}^{\infty}F_{n,\mathrm{c}}e^{-2A^2(2-A^2)\lambda_n^2 x^*}+\frac{4\gamma}{1+\gamma}\frac{2-\sigma_T}{\sigma_T Pr}Kn+\frac{3A^4-16A^2+24}{24(2-A^2)^2}} \tag{30}$$

where

$$F_{n,\mathrm{c}}=C_{n,\mathrm{c}}\left[\phi_n(A)-\frac{4}{A^2(2-A^2)}\int_0^A\left(1-Y^2\right)\phi_n(Y)Y\mathrm{d}Y\right] \tag{31}$$

$$x^*=\frac{x}{D_h Pe} \tag{32}$$

For PPM,

$$Nu(x)_{\mathrm{p}}=\frac{4}{\sum_{n=1}^{\infty}F_{n,\mathrm{p}}e^{-\lambda_n^2\frac{32x^*}{3A^3}}+\frac{8\gamma}{1+\gamma}\frac{2-\sigma_T}{\sigma_T Pr}Kn+\frac{2}{15A}+\frac{2}{105A^2}+\frac{1}{3}} \tag{33}$$

where

$$F_{n,\mathrm{p}}=C_{n,\mathrm{p}}\left[\phi_n\left(\frac{1}{A}\right)-\frac{3A^2}{2}\sum_{n=1}^{\infty}e^{-\lambda_n^2 X}\int_0^{\frac{1}{A}}\left(B-Y^2\right)\phi_n(Y)\mathrm{d}Y\right] \tag{34}$$

2.2 *Constant wall temperature*

When the wall temperature T_{w} is given, the non-dimensional boundary conditions for the energy equation are as follows

$$\theta(0,Y)=1 \tag{35}$$

$$\theta(\infty,Y)=\theta_\infty \tag{36}$$

$$\left.\frac{\partial\theta}{\partial Y}\right|_{Y=0}=0 \tag{37}$$

$$\theta\left(X,A^{2p-1}\right)=k\left.\frac{\partial\theta}{\partial Y}\right|_{Y=A^{2p-1}} \tag{38}$$

where k is defined as

$$k=-\frac{2^{3-p}A^{2p-1}\gamma}{1+\gamma}\frac{2-\sigma_T}{\sigma_T}\frac{Kn}{Pr} \tag{39}$$

Equations (37) and (38) are the second and third homogeneous boundaries respectively. The energy equation with this kind of boundary has a solution of the following form

$$\theta=\sum_{n=1}^{\infty}C_n e^{-\lambda_n^2 X}\phi_n(Y) \tag{40}$$

The eigenfunctions $\phi_n(Y)$ meet the following differential equation

$$-\left(B^{1-p}-Y^2\right)\lambda_n^2\phi_n=\frac{1}{Y^p}\frac{\mathrm{d}}{\mathrm{d}Y}\left(Y^p\frac{\mathrm{d}\phi_n}{\mathrm{d}Y}\right)+\frac{1}{Pe^2}\lambda_n^4\phi_n \quad (41)$$

and the corresponding boundary conditions are

$$\frac{d\phi_n}{dY}=0 \quad (42)$$

$$\phi_n\left(A^{2p-1}\right)-k\frac{d\phi_n}{dY}\bigg|_{Y=A^{2p-1}}=0 \quad (43)$$

Since the form of $\phi_n(Y)$ is similar to that under the constant heat flux, the Kummer equation can still be obtained through variable substitution, that is,

$$\eta\frac{\mathrm{d}^2\omega}{\mathrm{d}\eta^2}+\left(\frac{p+1}{2}-\eta\right)\frac{\mathrm{d}\omega}{\mathrm{d}\eta}+\left(B^{1-p}\lambda_n-p-1+\frac{\lambda_n^3}{Pe^2}\right)\frac{\omega}{4}=0 \quad (44)$$

Solving the boundary conditions will obtain the eigenvalues, which can be expressed as

$$\left(\frac{1}{A^{2p-1}\lambda_n k}+1\right)F(a,c,z)-\frac{4a}{1+p}F(a+1,c+1,z)=0 \quad (45)$$

C_n can be acquired by using the same procedure of that under the constant heat flux. Therefore, for CM, the local Nusselt number is

$$Nu(x)_{\mathrm{c}}=\frac{-A^3(2-A^2)\sum_{n=1}^{\infty}C_n\phi_n(X,A)e^{-2A^2\left(2-A^2\right)\lambda_n^2x^*}}{2k\sum_{n=1}^{\infty}C_ne^{-2A^2(2-A^2)\lambda_n^2x^*}\int_0^A(1-Y^2)\phi_nYdY} \quad (46)$$

For PPM, the local Nusselt number is

$$Nu(x)_{\mathrm{p}}=\frac{-8\sum_{n=1}^{\infty}C_n\phi_n(X,A)e^{-\frac{32}{3A^3}\lambda_n^2x^*}}{3kA^3\sum_{n=1}^{\infty}C_ne^{-\frac{32}{3A^3}\lambda_n^2x^*}\int_0^A(1-Y^2)\phi_nYdY} \quad (47)$$

3. Model validation

3.1 *Number of eigenvalues*

Note that there are infinite series in the expression of the local Nusselt number. But only limited eigenvalues need to be intercepted for the actual calculation. The number of eigenvalues that are a suitable compromise between the reasonable accuracy and solution cost needs to be determined. The number of eigenvalues mainly affects the local Nusselt number near the inlet, as shown in figure 3. When comparing the results in figure 3(a) and figure 3(b), it is found that the effect of N decreases as Kn increases. Because the entrance effect is not obvious when increasing the rarefaction effect. The maximum relative error between N = 15 and N = 20 in figure 3(a) is 0.44%, but the error between N = 15 and N = 20 in figure 3(c) is 3.37%, implying that the effect of N increases as Pe decreases. What's more, it is obvious that more eigenvalues are required to calculate $Nu(x)$ in CM from figure 3(a) and figure 3(d), and the maximum relative error between N = 20 and N = 25 in figure 3(d) is 1.58%. In this work, the first 20 eigenvalues are chosen to calculate $Nu(x)$.

3.2 *Validation of Gram–Schmidt orthogonalization*

In this work, the Gram–Schmidt orthogonalization was used to solve the heat transfer problem including the axial heat conduction. But the orthogonalization is an approximate method. The number of orthogonal functions needs to be determined during the orthogonalization. As the local Nusselt number can be obtained precisely when ignoring the axial heat conduction. We treated the analytical solution of Pe = ∞, Kn = 0 as a benchmark to verify the Gram–Schmidt orthogonalization, as shown in figure 4. What's more, Shah and London [3] also summarized the results of the local Nusselt number in PPM with constant heat flux, which are also used to verify the results. The number of the orthogonal function also mainly affects the local Nusselt number near the inlet. The results of Shah and London [3] and the benchmark solution are almost overlapped. The maximum relative error is 0.64% when comparing the results of 20 orthogonal functions with the benchmark solution or the data in Shah and London [3]. Therefore, 20 orthogonal functions are adopted in this work to enhance the calculation accuracy.

3.3 *Validation of analytic solutions*

It is essential to verify the analytic solutions before discussing the heat transfer characteristics further. For the extended Graetz problem in CM or PPM, there are some available data that can be compared with the present results as shown in figure 5. Figure 5(a) depicts the results in CM with Pe = ∞ under the constant heat flux. Obviously, the present results are consistent with that in Shah and London [3] and Haddout *et al* [13], but some deviations are found when compared with that in Ameel *et al* [6]. It can be ascribed to the difference in the number of eigenvalues because only 8 eigenvalues were employed in Ameel *et al* [6]. Figure 5(b) describes the variation of the local Nusselt number in CM and PPM with Kn = 0 under the constant wall temperature. The data in Chalhub *et al* [12] and Kalyoncu and Barisik [15] are also plotted to compare the results. Good agreements can be found and the maximum

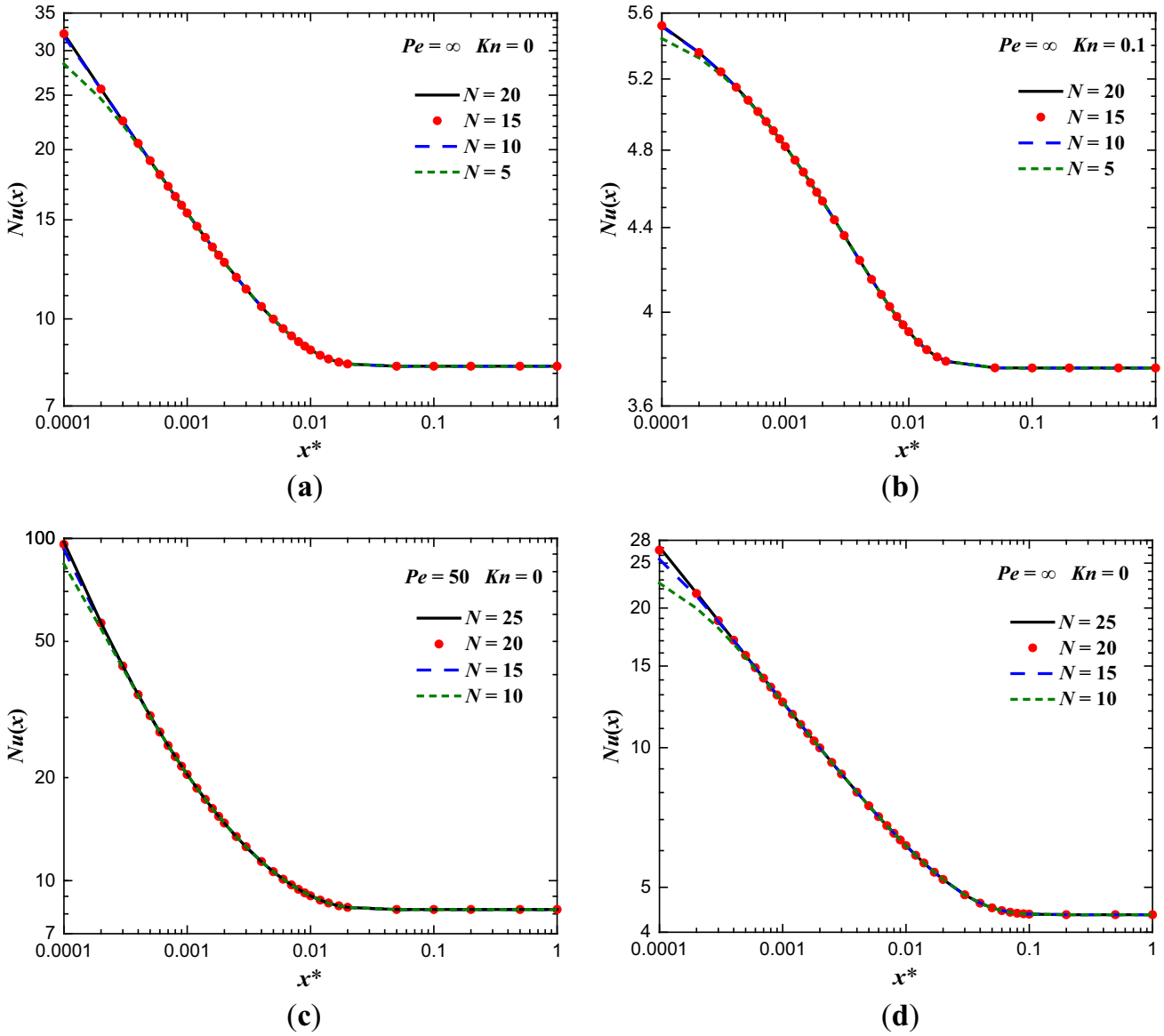

Figure 3. Effect of the number of eigenvalues on local Nusselt number with (**a**) $Pe = \infty$, $Kn = 0$, (**b**) $Pe = \infty$, $Kn = 0.1$, (**c**)$Pe = 50$, $Kn = 0$ in PPM; and with (**d**) $Pe = \infty$, $Kn = 0$ in CM.

relative errors between the present work and the literature data are less than 0.4% and 2% in PPM and CM, respectively.

4. Results and discussion

4.1 *Constant heat flux*

Figure 6 displays the influence of the rarefaction on the local Nusselt number. The rarefaction is directly proportional to the *Kn*. As expected, the Nusselt number decreases as *Kn* increases in both the entrance region and the fully developed region. The reduction is more apparent in the entrance region, indicating the entrance effect is greatly affected by the rarefaction. It is expected that the entrance effect will disappear if *Kn* is large enough. Because the gas is thinner with increasing *Kn*, which decreases the collision frequency between the gas molecules. While the axial conduction depends on the heat conduction between the gas molecules. Therefore, increasing *Kn* would weaken the heat transfer. Besides, the reduction is also distinct for low *Pe*. Since the axial heat conduction is significantly diminished when enhancing the rarefaction. The effect of the rarefaction on the heat transfer is more prominent in PPM when compared with that in CM, which maybe since the boundary conditions have more effect on the double-connected channel.

The influence of the axial heat conduction on the local Nusselt number is shown in figure 7. The results indicate

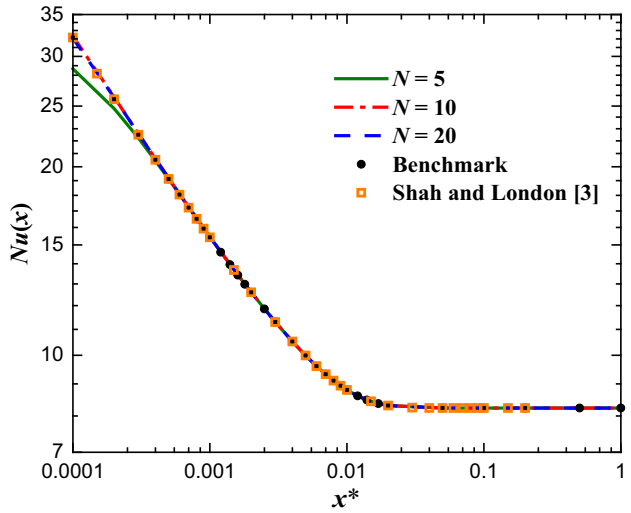

Figure 4. Effect of the number of the orthogonal function on local Nusselt number.

that $Nu(x)$ is inversely proportional to Pe, and the tendency is manifest when $Pe < 250$ with $Kn = 0$. The maximum relative error of $Nu(x)$ between $Pe = 500$ and $Pe = 1000$ are 3.1% and 0.08% when $Kn = 0$ and 0.1 respectively in CM, and for PPM they are 6.0% and 0.1% respectively. The influence of Pe can be thus omitted when $Pe>500$. Because the speed of the axial heat conduction is far slower than that of the heat convection if Pe is high enough, resulting in a small axial temperature gradient and the axial heat conduction can be omitted. Besides, the axial heat conduction only affects $Nu(x)$ at the entrance region and the effect gradually decreases along the streamwise direction. The fully developed Nusselt number is independent of Pe, which means the axial heat conduction only affects the local Nusselt number in the thermal entrance region [47]. It is worth noting that for the constant heat flux condition, the fluid temperature linear changes along the axial direction, which means the second derivative of the temperature along the axial direction can be ignored in the fully developed region. When comparing figure 7(a) and figure 7(b), it is obvious that the influence of Pe is greatly weakened as Kn increases. Similarly, the influence of Pe on $Nu(x)$ is more apparent in PPM in comparison with that in CM.

The above results reveal that due to the entrance effect, the heat transfer coefficient at the entrance region is much higher than that of the fully developed region. Therefore, it is necessary to determine the thermal entrance length to clarify the influence range of the entrance effect. Based on the definition of the thermal entrance length L^*_{th} [48], it can be calculated with the following expression

$$Nu(L^*_{th}) = 1.05Nu_\infty \tag{48}$$

where Nu_∞ is the fully developed Nusselt number.

The variation of the thermal entrance length is shown in figure 8. The symbol mark in the figure is the calculated value. The results in Shah and London [3], who gave the thermal entrance length of ignoring the axial heat conduction and rarefaction, are also used to make a contrast. The good result of the comparison supports the present work. Moreover, Colin [49] have summarized the thermal entry length without axial conduction for CM under constant heat flux boundary condition, and the results are also plotted in figure 8(b). The same trend can be found but some differences were also observed especially for low Kn. Note that the results in Colin [49] come from Ameel *et al* [6]. The

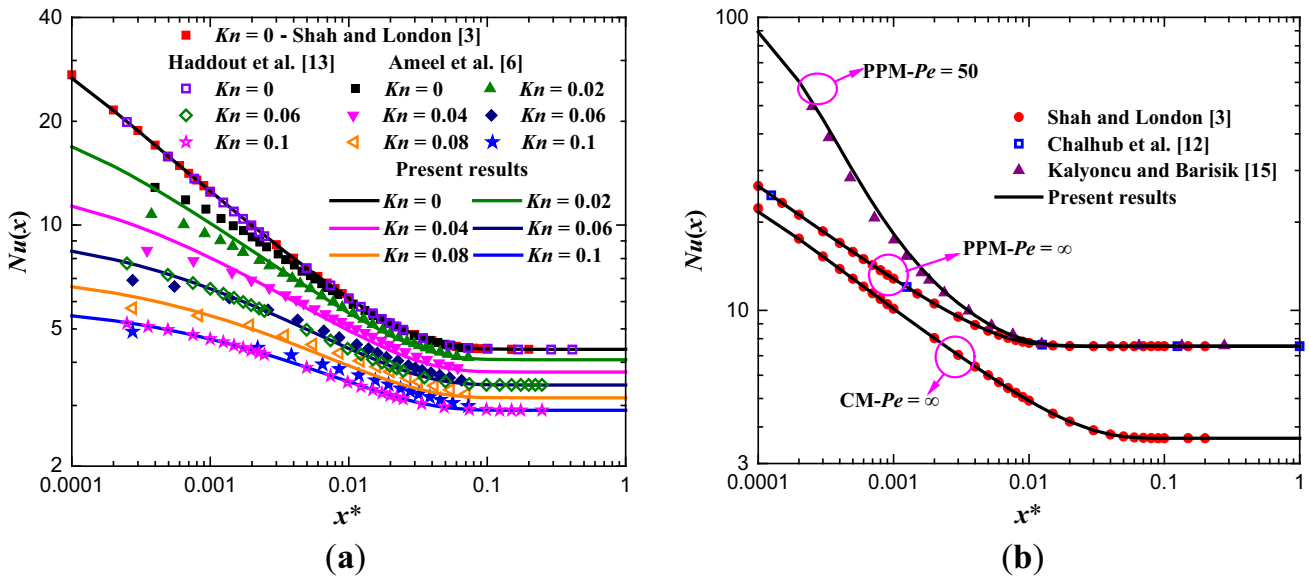

Figure 5. Validation of analytic solutions: (**a**) constant heat flux in CM and (**b**) constant wall temperature in CM and PPM.

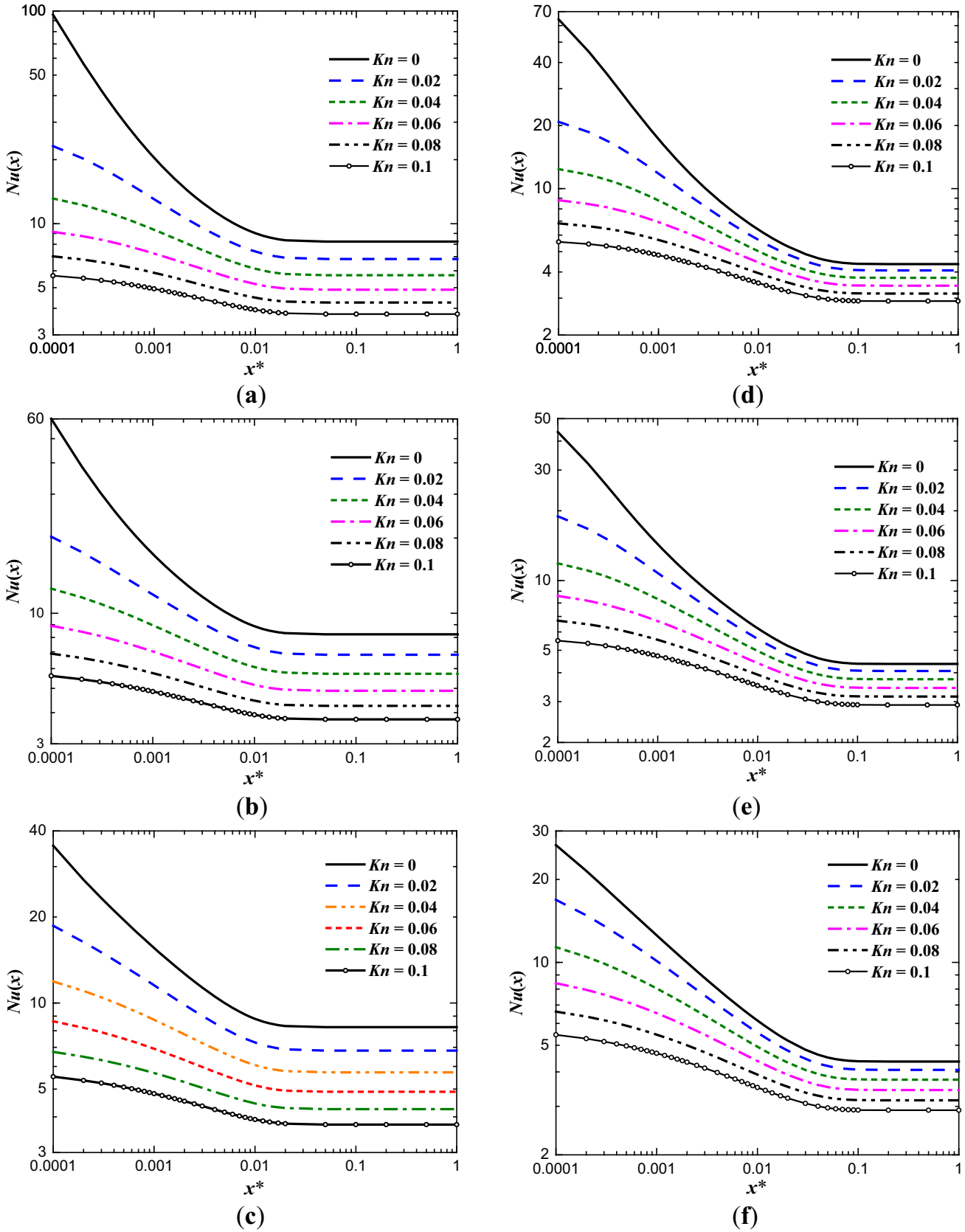

Figure 6. Effect of Kn on $Nu(x)$ in PPM with (**a**) $Pe = 50$ (**b**) $Pe = 100$ (**c**) $Pe = \infty$ and in CM with (**d**) $Pe = 50$, (**e**) $Pe = 100$ (**f**) $Pe = \infty$.

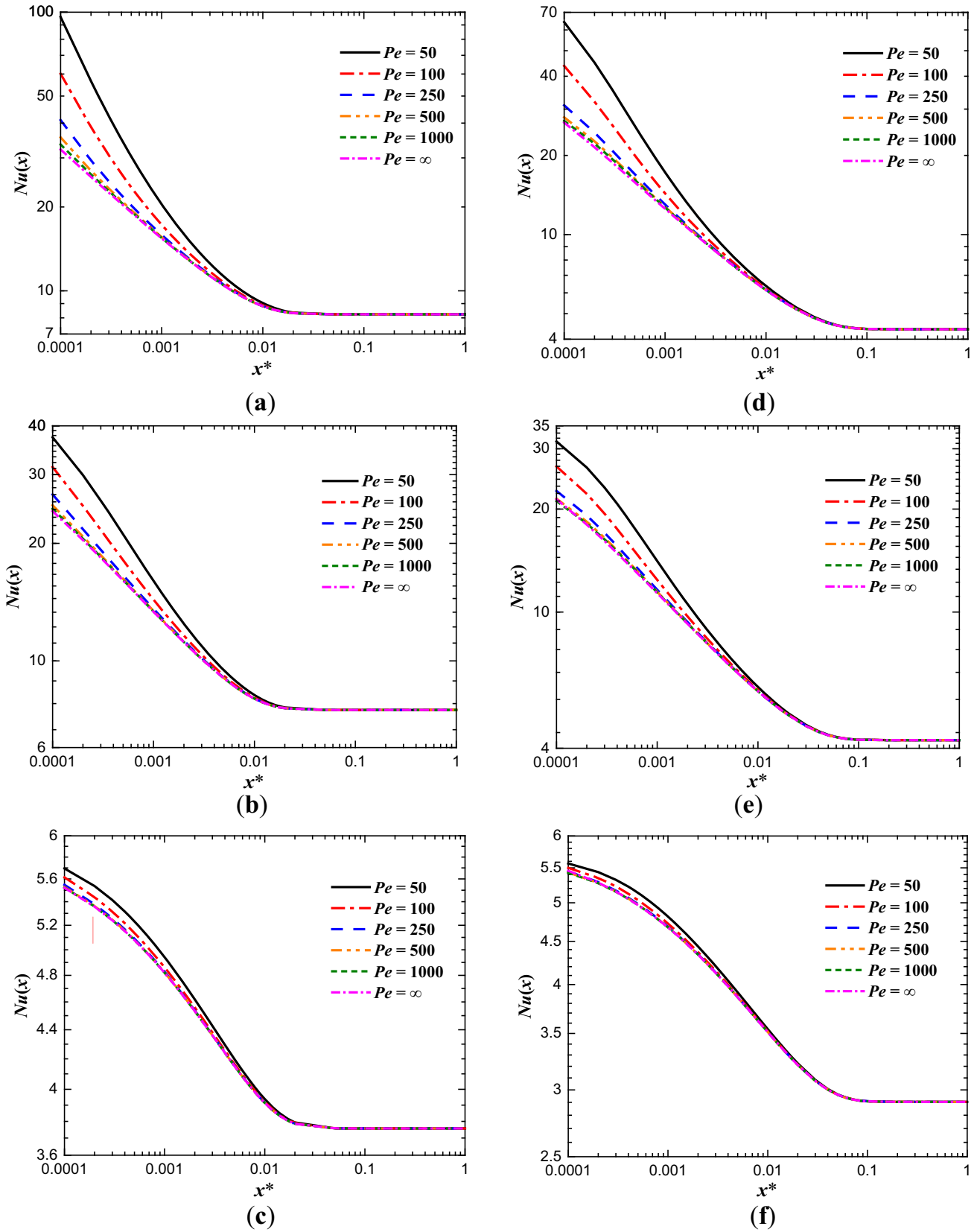

Figure 7. Effect of *Pe* on *Nu*(*x*) in PPM with (**a**) *Kn* = 0, (**b**) *Kn* = 0.01, (**c**) *Kn* = 0.1; and in CM with (**d**) *Kn* = 0, (**e**) *Kn* = 0.01, (**f**) *Kn* = 0.1.

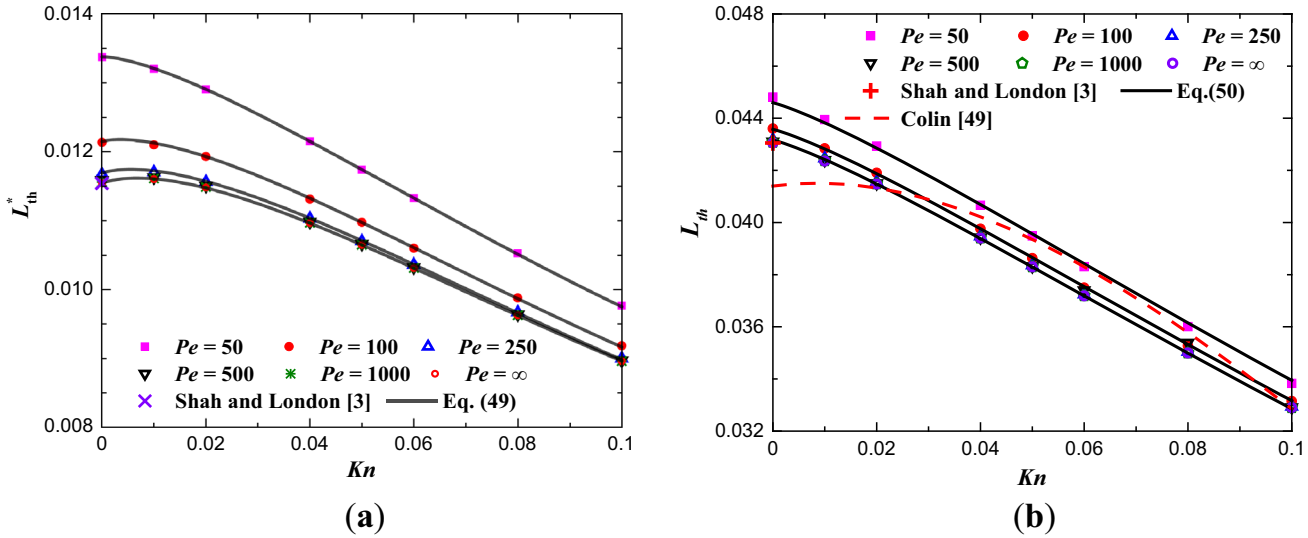

Figure 8. Variation of thermal entrance length in (**a**) PPM and (**b**) CM.

deviation can be ascribed to the fewer eigenvalues used in Ameel *et al* [6], as mentioned in section 3.3. While the Nusselt number at the entrance region is more sensitive to the number of the eigenvalue for low *Kn*. Despite this, the results in Ameel *et al* [6] or Colin [49] also verify our results because the relative error of the thermal entry length is within 3.8%. Besides, it is found that *Pe* has a distinct influence on the thermal entrance length when *Pe* is low. While the thermal entrance length hardly changes when $Pe > 500$. Note that the thermal entrance length increases for increasing fluid axial heat conduction (i.e., decreasing *Pe*). For example, in the case of the fluid heating situation, finite axial heat conduction would reduce the temperature of the fluid at any cross section, and hence a longer duct length would be required to achieve the fully developed temperature profile. In addition, the thermal entrance length, on the whole, decreases as *Kn* increases and the reduction is apparent for low *Pe*. When $0 \le Kn \le 0.1$ and $Pe \ge 50$, the correlations of the thermal entrance lengths are obtained by using the curve fitting. For PPM,

$$L^*_{\text{th}} = a + bKn + cKn^{1.5} + dKn^2 \tag{49}$$

The corresponding coefficients are shown in table 1. For CM,

Table 1. Coefficients in Eq. (49).

Pe	*a*	*b*	*c*	*d*
50	0.0134	0.00550	−0.265	0.420
100	0.0122	0.0260	−0.330	0.485
250	0.0117	0.0330	−0.345	0.490
>500	0.0115	0.0384	−0.369	0.525

$$L^*_{\text{th}} = \left(-0.5913 + 0.5967Kn + 5.044Kn^{1.5} - 7.796Kn^2\right)\left(-0.073 - 2.767Pe^{-1.8}\right) \tag{50}$$

The results of the Eqs. (49) and (50) are shown by the solid line in figure 8 and good agreements can be found between the correlations and the calculated values.

4.2 *Constant wall temperature*

The influence of *Kn* on *Nu*(*x*) with the constant wall temperature is shown in figure 9. Similar to the results under the constant heat flux, *Nu*(*x*) is a decreasing function of *Kn*. As *Kn* increases, the collision frequency between the gas molecules becomes weak. And the entrance effect is greatly affected by *Kn*, especially for low *Pe*, which is due to the fact that the axial conduction enhances the entrance effect and the effect of the rarefaction is more evident. The influence of the rarefaction on the heat transfer performance is more obvious in PPM compared with that in CM.

The influence of the axial heat conduction on the local Nusselt number is shown in figure 10. The local Nusselt number increases as *Pe* decreases, especially when $Pe < 250$. The maximum relative error of *Nu*(*x*) between $Pe = 100$ and $Pe = 500$ are 36.2%, 15.5%, and 1.6% in CM when $Kn = 0$, 0.02, and 0.1 respectively, indicating the effect of the axial conduction is obvious when $Pe > 100$, especially for low *Kn*. And the maximum relative error of *Nu*(*x*) between $Pe = 500$ and $Pe = 1000$ in CM are 3.3%, 1.5%, and 0.1% when $Kn = 0$, 0.02, and 0.1 respectively, and for PPM they are 6.9%, 1.8% and 0.1% respectively. Therefore, when $Pe > 100$, the effect of the axial heat conduction on the entrance effect cannot be ignored in the slip regime until $Pe > 500$, rather than $Pe > 100$

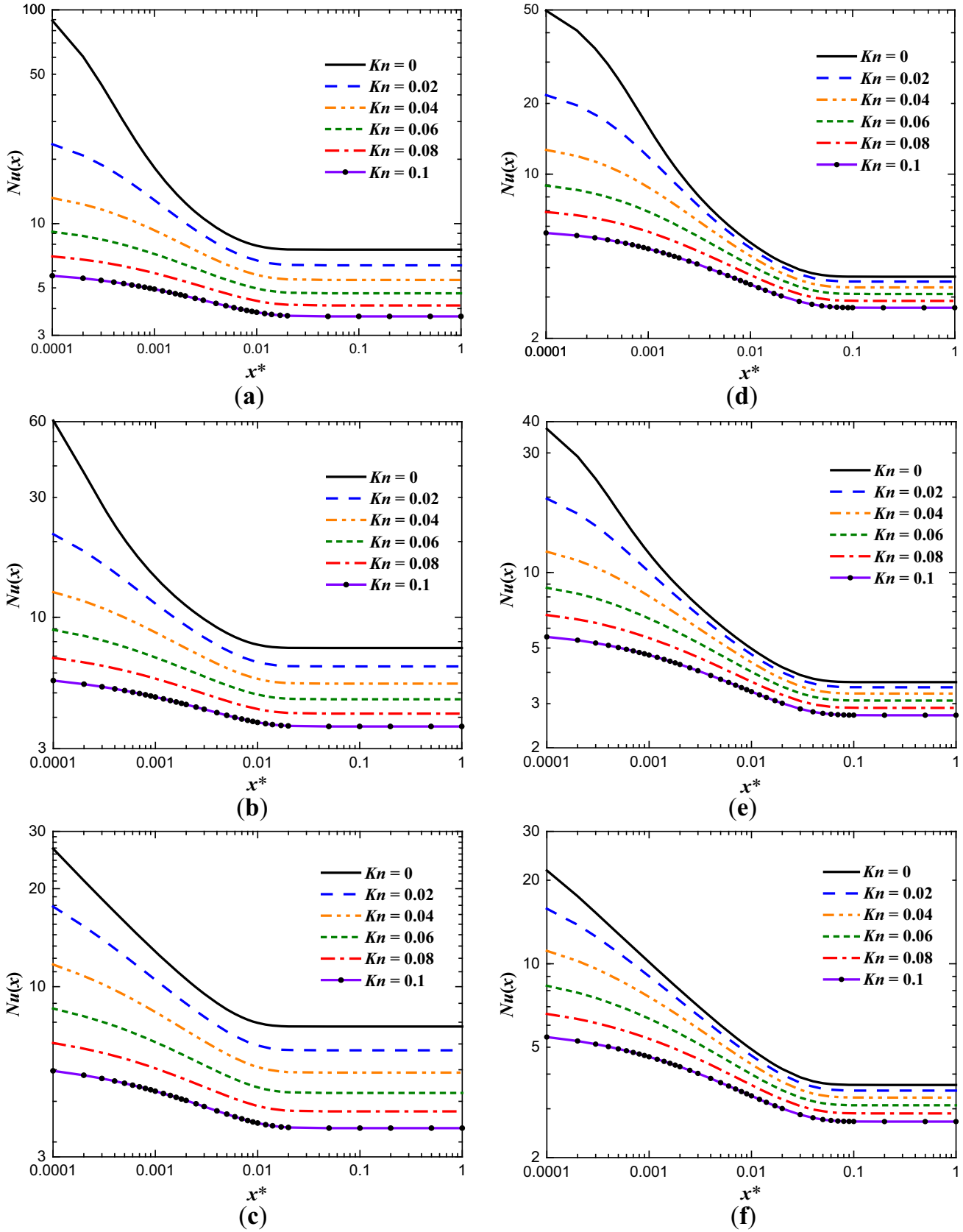

Figure 9. Effect of *Kn* on *Nu*(*x*) in PPM with (**a**) *Pe* = 50, (**b**) *Pe* = 100, (**c**) *Pe* = ∞; and in CM with (**d**) *Pe* = 50, (**e**) *Pe* = 100, (**f**) *Pe* = ∞.

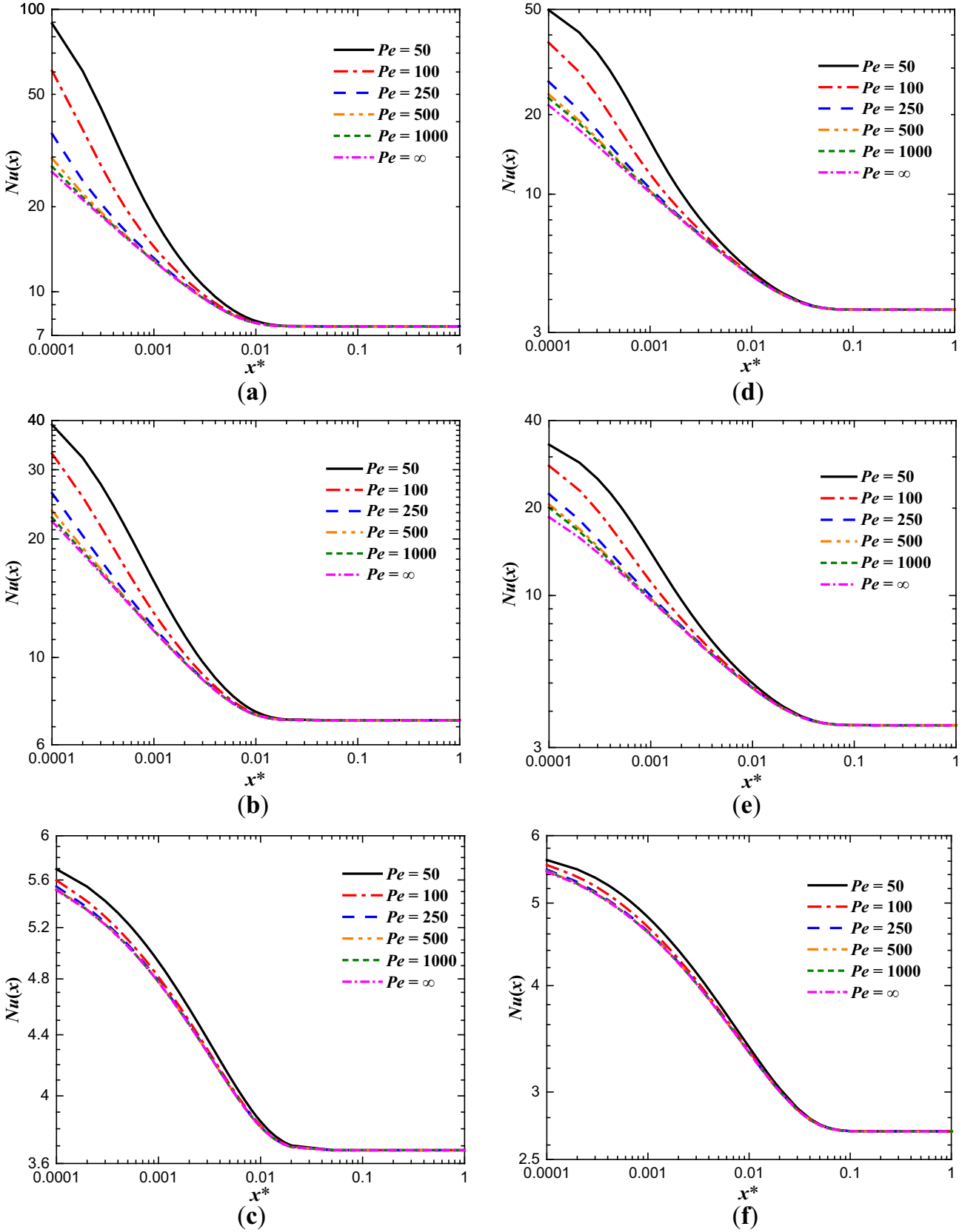

Figure 10. Effect of *Pe* on *Nu*(*x*) in PPM with (**a**) *Kn* = 0, (**b**) *Kn* = 0.01, (**c**) *Kn* = 0.1 and in CM with (**d**) *Kn* = 0, (**e**) *Kn* = 0.01 and (**f**) *Kn* = 0.1.

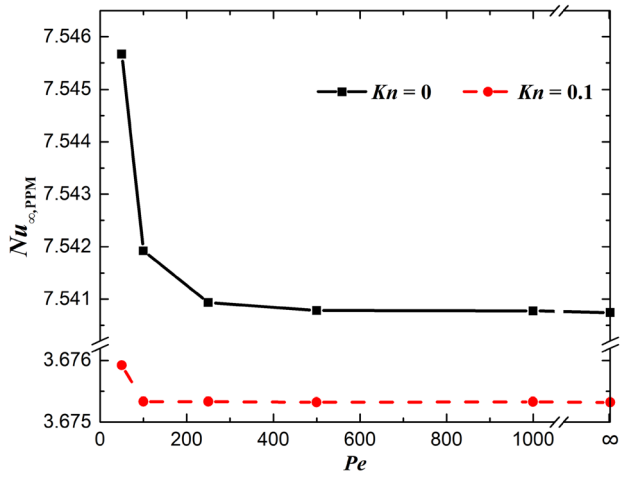

Figure 11. Variation of the fully developed *Nu* with *Pe* in PPM.

in the existing literature. Likewise, the influence of the axial heat conduction attenuates as *Kn* increases. Besides, the influence is more obvious in PPM in comparison with that in CM. But the difference decreases as *Kn* increases, indicating that increasing *Kn* would downgrade the effect of the channel shape on the heat transfer.

The influence of *Pe* on $Nu(x)$ gradually decreases along the streamwise direction. But it is worth noting that *Pe* has an influence on Nu_∞ under the constant wall temperature, as shown in figure 11. Since the fully developed Nusselt number with the constant wall temperature strongly depends on the first eigenvalue, which is affected by both *Kn* and *Pe*. However, the effect of *Pe* on Nu_∞ is small when $Pe \geq 50$, and the effect decreases as *Kn* increases.

Table 2. Coefficients in Eq. (51).

Pe	*a*	*b*	*c*	*d*
50	0.00945	0.0543	0.0489	−1.463
100	0.00845	0.0430	0.1160	−1.390
250	0.00808	0.0315	0.2600	−1.960
>500	0.00798	0.0298	0.2860	−2.056

The effects of *Pe* and *Kn* on the thermal entrance length are shown in figure 12. Different from the results under the constant heat flux, the thermal entrance length increases first and then decreases as *Kn* increases. The peak values of L^*_{th} arise when *Kn* is 0.4 or 0.5. L^*_{th} is gradually getting shorter as *Pe* increases and almost keeps unchanged when $Pe > 500$. Besides, L^*_{th} of CM is about 3–4 times that of PPM. This is because two surfaces are in contact with the fluid in PPM, the thermal boundary layer is thus formed faster and shortens L^*_{th}. When $0 \leq Kn \leq 0.1$ and $Pe \geq 50$, the correlations of L^*_{th} are obtained by using the curve fitting. For PPM,

$$L^*_{th} = a + bKn + cKn^{1.5} + dKn^2 + eKn^{2.5} \qquad (51)$$

The corresponding coefficients are shown in table 2. For CM,

$$L^*_{th} = \left(-0.0665 + 0.0038Kn - 0.9Kn^{1.5} + 4.29Kn^2 - 4.14Kn^{2.5}\right)\left(-0.504 - 33.33Pe^{-1.83}\right) \qquad (52)$$

The results of the Eqs. (51) and (52) are shown by the solid line in figure 12 and a high degree of coincidence can be found between the correlations and the calculated values.

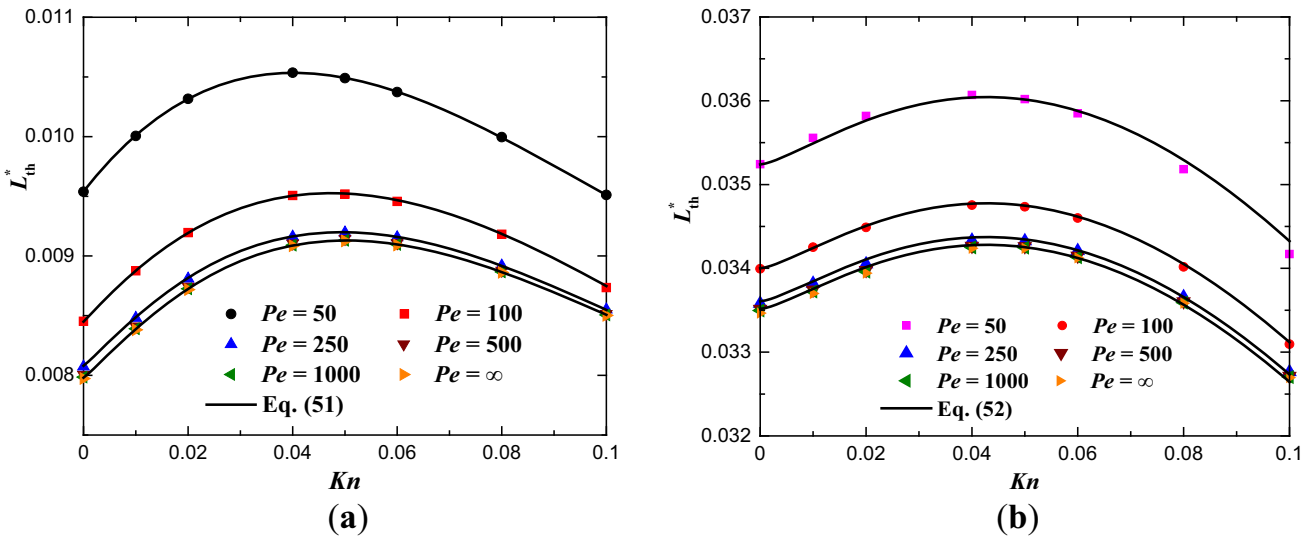

Figure 12. Variation of thermal entrance length in (**a**) PPM and (**b**) CM.

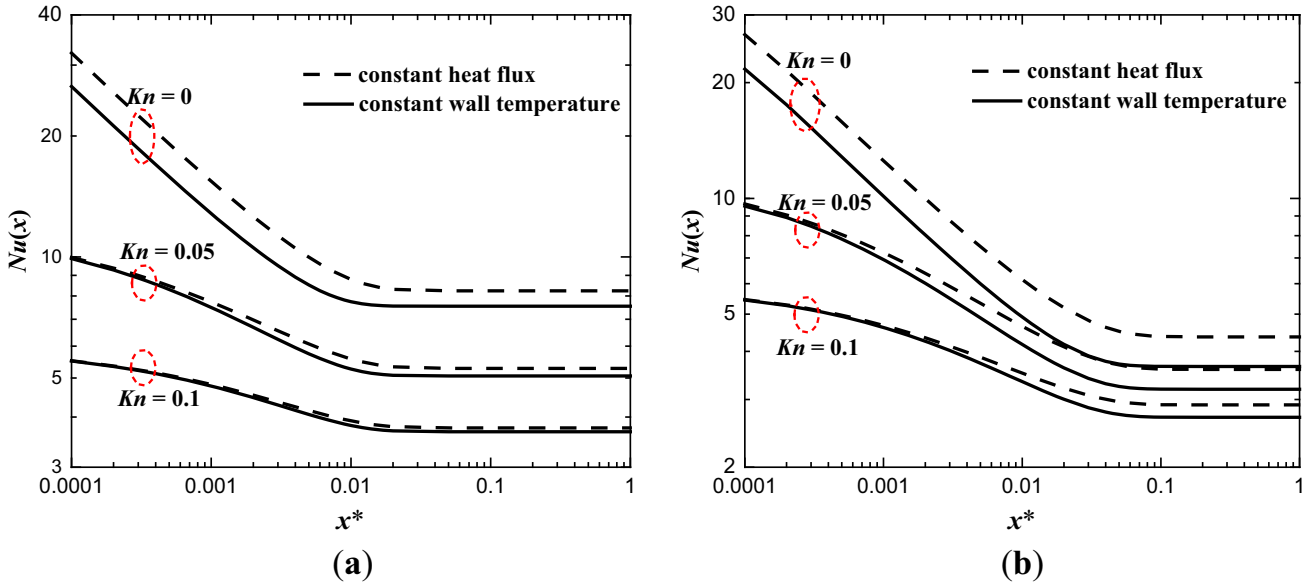

Figure 13. Effect of *Kn* on *Nu*(*x*) under different boundary conditions in (**a**) PPM, and (**b**) CM.

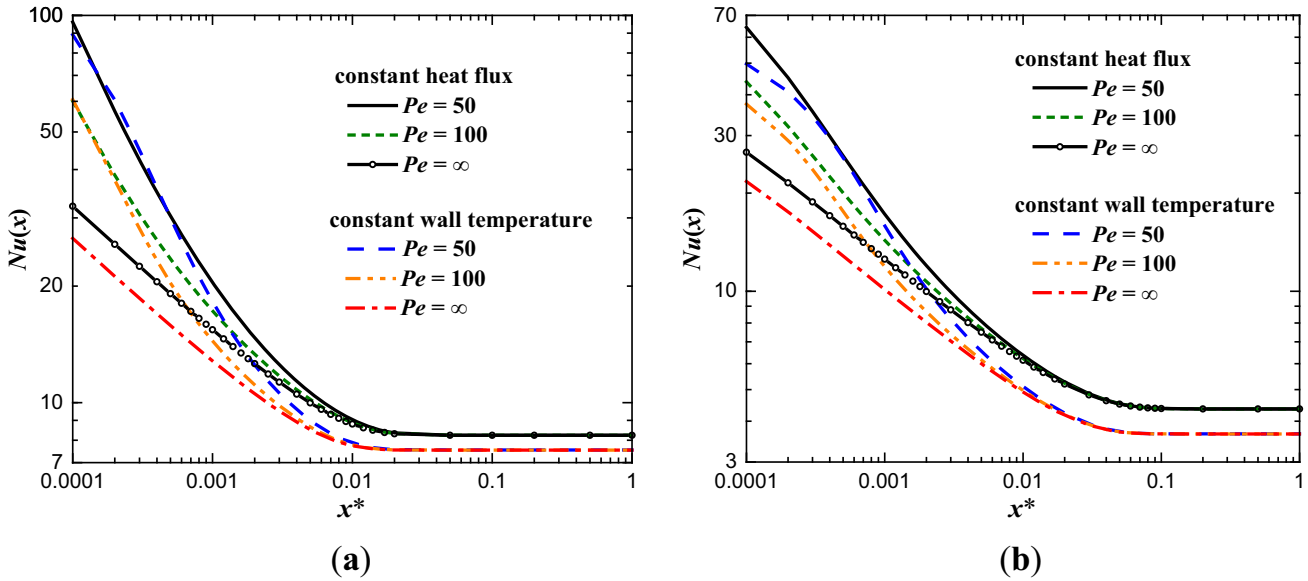

Figure 14. Effect of *Pe* on *Nu*(*x*) under different boundary conditions in (**a**) PPM and (**b**) CM.

4.3 *Comparison of heat transfer under different thermal boundaries*

Figure 13 plots the influence of the rarefaction on the local Nusselt number in PPM and CM with different boundary conditions. The rarefaction effect has almost the same effect on the local Nusselt number in the two microchannels. Taking the results in PPM as an example, the local Nusselt number decreases significantly with the increase of *Kn* under the two thermal boundaries. When *Kn* = 0, the curves of *Nu*(*x*) with the two boundary conditions are almost parallel. As *Kn* increases, the two curves have an intersection or even almost overlap at the entrance region. The difference of the local Nusselt number with the two boundary conditions almost disappears when *Kn* = 0.1 in CM. But the difference is still obvious in the fully developed region in PPM, indicating the effect of the thermal boundary condition on the heat transfer performance is more important in PPM. The result indicates that the rarefaction effect would diminish the difference in the heat

transfer performance between the two boundaries. At the same time, the result demonstrates the change of Kn has a greater influence on the heat transfer under the constant heat flux when compared with that under the other boundary.

In figure 14, the effect of the axial heat conduction on the heat transfer is depicted in PPM and CM with different boundary conditions. When the axial heat conduction is not considered, that is, $Pe \to \infty$, the heat transfer coefficient with the constant wall temperature is always lower. As Pe decreases, $Nu(x)$ under the constant wall temperature tends to exceed that under the constant heat flux. The phenomenon shows that the axial heat conduction would greatly enhance the heat transfer performance at the entrance region, especially for the constant wall temperature. In addition, it can be found that there is a fluctuation for $Nu(x)$ near the inlet when $Pe = 50$ under the constant wall temperature boundary, which indicates that more eigenvalues are needed to calculate more accurate results for this case. While adding an eigenvalue will double the amount of calculation, so using the numerical methods to obtain the heat transfer coefficient of small Pe may reduce the cost.

5. Conclusions

In this paper, the energy equations of the thermally developing flow in circular and parallel plates microchannels are solved by using the separated variable method combined with the Kummer function and Gram-Schmidt orthogonalization. The temperature distribution is obtained, and the expression of the dimensionless heat transfer coefficient is derived. By analyzing the influence of the axial heat conduction and the rarefaction on the heat transfer characteristic in microchannels with two boundary conditions, the following conclusions are drawn:

(1) The number of eigenvalues mainly affects the results near the inlet. With increasing Kn and Pe, the entrance effect is not obvious and the effect of the number of eigenvalues on the Nusselt number decreases as well. More eigenvalues are needed to accurately calculate the local Nusselt number in CM comparatively with that in PPM. Besides that, more eigenvalues are required to obtain the local Nusselt number accurately for the constant wall temperature boundary condition when compared with that for the constant heat flux.
(2) Considering the axial heat conduction will enhance the heat transfer capacity at the entrance region, especially when $Pe < 50$. While the maximum relative errors of $Nu(x)$ between $Pe = 500$ and $Pe = 1000$ in CM and PPM are within 7%, even within 0.1% for $Kn = 0.1$. The effect of axial heat conduction on Nu can be thus ignored when $Pe > 500$. In the fully developed region, the axial heat conduction does not affect the Nusselt number under the constant heat flux but still has a small influence on the heat transfer under the constant wall temperature. In addition, enhancing the rarefaction would weaken the entrance effect and then weaken the influence of axial heat conduction on the heat transfer as well.
(3) The thermal entrance length decreases with the increase of Kn under the constant heat flux, but it increases first and then decreases as Kn increases under the constant wall temperature. The thermal entrance length decreases as the axial fluid heat conduction fades away. Besides, the thermal entrance length in CM is 3–4 times that of PPM because PPM can be treated as a double-connected channel. Finally, the correlations of the thermal entrance length are proposed.
(4) The influence of thermal boundary conditions on the heat transfer coefficient decreases as increasing Kn. Considering these two boundary conditions, the rarefaction effect has more influence on the heat transfer under the constant heat flux, and the effect of the axial heat conduction on the heat transfer is more apparent under the constant wall temperature.

Appendix A: Steps of Gram-Schmidt orthogonalization to obtain C_n

For the eigenfunctions sequence $\{\phi_n\}$, assuming that the orthogonalized function sequences are $\{g_n\}$, the relationship between the above two is as follows

$$g_1 = \phi_1 \tag{A-1}$$

$$g_2 = \phi_2 - a_{21}g_1 = \phi_2 - a_{21}\phi_1 \tag{A-2}$$

$$\begin{aligned} g_3 = \phi_3 - a_{32}g_2 - a_{31}g_1 &= \phi_3 - a_{32}(\phi_2 - a_{21}\phi_1) - a_{31}\phi_1 \\ &= \phi_3 - a_{32}\phi_2 + (a_{32}a_{21} - a_{31})\phi_1 \end{aligned} \tag{A-3}$$

$$g_n = \phi_n - \sum_{m=1}^{n-1} a_{nm}g_m \tag{A-4}$$

For the orthogonal function sequences $\{g_n\}$, there is the following orthogonal property when $i \neq j$

$$\int_0^1 g_i g_j \mathrm{d}Y = 0 \tag{A-5}$$

Substituting (A-1) and (A-2) into (A-5) yields

$$\begin{aligned} \int_0^1 g_1 g_2 \mathrm{d}Y &= \int_0^1 \phi_1(\phi_2 - a_{21}g_1)\mathrm{d}Y \\ &= \int_0^1 \phi_1\phi_2 \mathrm{d}Y - a_{21}\int_0^1 \phi_1 g_1 \mathrm{d}Y = 0 \end{aligned} \tag{A-6}$$

then

$$a_{21} = \frac{\int_0^1 \phi_1 \phi_2 \mathrm{d}Y}{\int_0^1 \phi_1 g_1 \mathrm{d}Y} = \frac{<\phi_1, \phi_2>}{<\phi_1, g_1>} \qquad (\mathrm{A}-7)$$

More generally,

$$a_{nm} = \frac{<\phi_n, g_m>}{<g_m, g_m>} \qquad (\mathrm{A}-8)$$

Based on the inlet boundary condition, setting the coefficient of the eigenfunctions after the orthogonalization is B_n, namely

$$\sum_{n=1}^{\infty} C_n \phi_n(Y) = \sum_{n=1}^{\infty} B_n g_n(Y) \qquad (\mathrm{A}-9)$$

and

$$\sum_{n=1}^{\infty} B_n g_n(Y) = \theta(0, Y) \qquad (\mathrm{A}-10)$$

The coefficient B_n can be obtained based on the characteristics of the orthogonal function:

$$B_n = \frac{\int_0^{1/A} \theta(0, Y) g_n \mathrm{d}Y}{\int_0^{1/A} g_n^2 \mathrm{d}Y} \qquad (\mathrm{A}-11)$$

According to (A-1)–(A-4), we have

$$\begin{aligned}\sum_{n=1}^{\infty} B_n g_n(Y) = {} & B_1\phi_1 + B_2(\phi_2 - a_{21}\phi_1) + B_3(\phi_3 - a_{32}\phi_2 \\ & + a_{32}a_{21}\phi_1 - a_{31}\phi_1) + B_4(\phi_4 - a_{43}\phi_3 + a_{43}a_{32}\phi_2 \\ & - a_{43}a_{32}a_{21}\phi_1 + a_{43}a_{31}\phi_1 - a_{42}\phi_2 + a_{42}a_{21}\phi_1 - a_{41}\phi_1) \\ & + \cdots B_n\left(\phi_n - \sum_{m=1}^{m-1} a_{nm} g_m\right)\end{aligned} \qquad (\mathrm{A}-12)$$

After determining B_n, C_n can be calculated according to (A-9), that is

$$\begin{aligned} C_1 &= B_1 - B_2 k_{1,2} - \cdots - B_N k_{1,N} = B_1 - \sum_{i=n+1}^{N} B_i k_{1,i} \\ &\vdots \\ C_n &= B_n - B_{n+1} k_{n,n+1} - \cdots - B_N k_{n,N} = B_n - \sum_{i=n+1}^{N} B_i k_{n,i} \\ &\vdots \\ C_N &= B_N \end{aligned} \qquad (\mathrm{A}-13)$$

where

$$\begin{aligned} k_{n,m} &= a_{m,n} k_{n,n} - a_{m,n+1} k_{n,n+1} - \cdots - a_{m,m-1} k_{n,m-1} = a_{m,n} \\ &\quad - \sum_{i=n+1}^{m-1} a_{m,i} k_{n,i} \\ k_{n,n} &= 1 \end{aligned} \qquad (\mathrm{A}-14)$$

List of symbols

c_p	Specific heat (J kg^{-1} K^{-1})
C_n	Coefficient in Eq. (16)
D_h	Hydraulic diameter (m)
h	Convective heat transfer coefficient (W m^{-2} K^{-1})
k	Parameter defined by Eq. (39)
Kn	Knudsen number
Kn_u	Modified Knudsen number = $Kn(2–\sigma_v)/\sigma_v$
Nu	Nusselt number
p	Geometry parameter
Pe	Peclet number
Pr	Prandtl number
Q	Internal heat generation (W m^{-3})
q	Heat flux (W m^{-2})
r	R-Coordinate (m)
T	Temperature (K)
u	Fluid velocity (m s^{-1})
x	X-Coordinate (m)
x^*	Non-dimensional length = $x/(D_h Pe)$
y	Y-Coordinate (m)

Greek symbols

β	Coefficient of thermal expansion (K^{-1})
γ	Ratio of specific heats
θ	Dimensionless temperature
κ	Fluid thermal conductivity (W m^{-1} K^{-1})
λ	Mean free path (m)
λ_n^2	Eigenvalue
μ	Dynamic viscosity (N s m^{-2})
ρ	Fluid density (kg m^{-3})
σ_v	Tangential momentum accommodation coefficient
σ_T	Thermal accommodation coefficient
Φ	Viscous dissipation function
ϕ_n	Eigenfunction

Subscripts

∞	Fully developed region
c	Microtube
m	Mean
p	Parallel plates microchannel
w	Wall
in	Inlet

Abbreviation

CM Circular microchannel
PPM Parallel plates microchannel

Acknowledgements

This research was supported by the Talents Special Fund of China Three Gorges University (No. 8210403).

References

[1] Agrawal A, Kushwaha H M and Jadhav R S 2020 Microscale flow and heat transfer. Springer International Publishing, Cham
[2] Bennett T D 2019 Correlations for the Graetz problem in convection – Part 1: for round pipes and parallel plates. *Int. J. Heat Mass Transf.* 136: 832–841
[3] Shah R K and London A L 1978 *Laminar flow forced convection in ducts, Suppl. l, Advanced Heat Transfer*. New York: Academic Press
[4] Barron R F, Wang X, Ameel T and Warrington R O 1997 The Graetz problem extended to slip-flow. *Int. J. Heat Mass Transf.* 40(8): 1817–1823
[5] Barron R F, Wang X, Warrington R O and Ameel T A 1996 Evaluation of the eigenvalues for the graetz problem in slip-flow. *Int. Commun. Heat Mass Transf.* 23(4): 563–574
[6] Ameel T A, Wang X, Barron R F and Warrington R O 1997 Laminar forced convection in a circular tube with constant heat flux and slip flow. *Microsc. Thermophys. Eng.* 1(4): 303–320
[7] Larrode F E, Housiadas C and Drossinos Y 2000 Slip-flow heat transfer in circular tubes. *Int. J. Heat Mass Transf.* 43: 2669–2680
[8] Tunc G and Bayazitoglu Y 2001 Heat transfer in microtubes with viscous dissipation. *Int. J. Heat Mass Transf.* 44(13): 2395–2403
[9] Xu F and Ma H 2012 Analytical solution of the Graetz problem extended to slip-flow in microtube. *J. Heat Transf.* 134(10): 2–3
[10] Duan Z and He B 2014 Extended Reynolds analogy for slip and transition flow heat transfer in microchannels and nanochannels. *Int. Commun. Heat Mass Transf.* 56: 25–30
[11] Hooman K, Li J and Dahari M 2016 Slip flow forced convection through microducts of arbitrary cross-section: Heat and momentum analogy. *Int. Commun. Heat Mass Transf.* 71: 176–179
[12] Chalhub D J N M, Sphaier L A and Alves L S D B 2016 Integral transform solution for thermally developing slip-flow within isothermal parallel plates. *Comput. Therm. Sci.* 8(2): 147–161
[13] Haddout Y, Essaghir E, Oubarra A and Lahjomri J 2018 Convective heat transfer for a gaseous slip flow in micropipe and parallel-plate microchannel with uniform wall heat flux: effect of axial heat conduction. *Indian J. Phys.* 92(6): 741–755
[14] Lahjomri J, Oubarra A and Alemany A 2002 Heat transfer by laminar Hartmann flow in thermal entrance eregion with a step change in wall temperatures: the Graetz problem extended. *Int. J. Heat Mass Transf.* 45(5): 1127–1148
[15] Kalyoncu G and Barisik M 2016 The extended Graetz problem for micro-slit geometries; analytical coupling of rarefaction, axial conduction and viscous dissipation. *Int. J. Therm. Sci.* 110: 261–269
[16] Saha S K, Agrawal A and Soni Y 2017 Heat transfer characterization of rhombic microchannel for H1 and H2 boundary conditions. *Int. J. Therm. Sci.* 111: 223–233
[17] Kuddusi L and Cetegen E 2009 Thermal and hydrodynamic analysis of gaseous flow in trapezoidal silicon microchannels. *Int. J. Therm. Sci.* 48(2): 353–362
[18] Tso C P, Sheela-Francisca J and Hung Y M 2010 Viscous dissipation effects of power-law fluid flow within parallel plates with constant heat fluxes. *J. Non-Newtonian Fluid Mech.* 165(11–12): 625–630
[19] Chen S 2010 Lattice Boltzmann method for slip flow heat transfer in circular microtubes: Extended Graetz problem. *Appl. Math. Comput.* 217(7): 3314–3320
[20] Hong C, Asako Y and Suzuki K 2011 Heat transfer characteristics of gaseous slip flow in concentric micro-annular tubes. *J. Heat Transf.* 133
[21] Kabar Y, Bessaïh R and Rebay M 2013 Conjugate heat transfer with rarefaction in parallel plates microchannel. *Superlattice Microst.* 60: 370–388
[22] Loussif N and Orfi J 2014 Simultaneously developing laminar flow in an isothermal micro-tube with slip flow models. *Heat Mass Transf.* 50: 573–582
[23] Haase A S, Chapman S J, Tsai P A, Lohse D and Lammertink R G 2015 The Graetz–Nusselt problem extended to continuum flows with finite slip. *J. Fluid Mech.* 764
[24] Kumar R and Mahulikar S P 2021 Effect of density variation on rarefied and non-rarefied gaseous flows in developing region of microtubes. *Iranian J. Sci. Technol. Trans. Mech. Eng.* 45(2): 415–425
[25] Şen S 2019 Numerical investigation of the effect of second order slip flow conditions on interfacial heat transfer in micro pipes. *Sadhana – Acad. Proceed. Eng. Sci.* 44(7)
[26] Saghafian M, Saberian I, Rajabi R and Shirani E 2015 A numerical study on slip flow heat transfer in micro-poiseuille flow using perturbation method. *J. Appl. Fluid Mech.* 8(1): 123–132
[27] Yu F, Wang T and Zhang C 2018 Effect of axial conduction on heat transfer in a rectangular microchannel with local heat flux. *J. Therm. Sci. Technol.* 13(1): 1–13
[28] Hemadri V, Biradar G S, Shah N, Garg R, Bhandarkar U V and Agrawal A 2018 Experimental study of heat transfer in rarefied gas flow in a circular tube with constant wall temperature. *Exp. Therm. Fluid Sci.* 93: 326–333
[29] Tada S and Ichimiya K 2007 Numerical simulation of forced convection in a porous circular tube with constant wall heat flux: An extended Graetz problem with viscous dissipation. *Chem. Eng. Technol.* 30(10): 1362–1368
[30] Renksizbulut M and Niazmand H 2016 Laminar flow and heat transfer in the entrance region. *J. Heat Transf.* 128: 63–74
[31] Avci M and Aydin O 2018 Analysis of extended micro-Graetz problem in a microtube. *Sadhana – Acad. Proceed. Eng. Sci.* 43(7): 1–9

[32] Barişik M, Yazicioğlu A G, Çetin B and Kakaç S 2015 Analytical solution of thermally developing microtube heat transfer including axial conduction, viscous dissipation, and rarefaction effects. *Int. Commun. Heat Mass Transf.* 67: 81–88

[33] Telles A S, Queiroz E M and Elmôr Filho G 2001 Solutions of the extended Graetz problem. *Int. J. Heat Mass Transf.* 44(2): 471–483

[34] Jambal O, Shigechi T, Davaa G and Momoki S 2005 Effects of viscous dissipation and fluid axial heat conduction on heat transfer for non-Newtonian fluids in ducts with uniform wall temperature: Part I: Parallel plates and circular ducts. *Int. Commun. Heat Mass Transf.* 32(9): 1165–1173

[35] Renksizbulut M, Niazmand H and Tercan G 2006 Slip-flow and heat transfer in rectangular microchannels with constant wall temperature. *Int. J. Therm. Sci.* 45(9): 870–881

[36] Jeong H E and Jeong J T 2006 Extended Graetz problem including axial conduction and viscous dissipation in microtube. *J. Mech. Sci. Technol.* 20(1): 158–166

[37] Myong R S, Lockerby D A and Reese J M 2006 The effect of gaseous slip on microscale heat transfer: An extended Graetz problem. *Int. J. Heat Mass Transf.* 49(15–16): 2502–2513

[38] Hettiarachchi H D M, Golubovic M, Worek W M and Minkowycz W J 2008 Three- dimensional laminar slip-flow and heat transfer in a rectangular microchannel with constant wall temperature. *Int. J. Heat Mass Transf.* 51(21–22): 5088–5096

[39] van Rij J, Ameel T and Harman T 2009 The effect of viscous dissipation and rarefaction on rectangular microchannel convective heat transfer. *Int. J. Therm. Sci.* 48: 271–281

[40] Saghafian M, Saberian I, Rajabi R and Shirani E 2015 A numerical study on slip flow heat transfer in micro-poiseuille flow using perturbation method. *J. Appl. Fluid Mech.* 8: 123–132

[41] Loussif N and Orfi J 2015 Slip flow heat transfer in microtubes with viscous dissipation. *Desalin. Water Treat.* 53: 1263–1274

[42] Ramadan K M, Kamil M and Bataineh M S 2019 Conjugate heat transfer in a microchannel simultaneously developing gas flow: a vorticity stream function-based numerical analysis. *J. Therm. Sci. Eng. Appl.* 11

[43] Sun Q, Choi K S and Mao X 2020 An analytical solution of convective heat transfer in microchannel or nanochannel. *Int. Commun. Heat Mass Transf.* 117: 104766

[44] Bejan A 2013 Convection Heat Transfer. John Wiley and Sons, New York

[45] Duan Z and He B 2018 Further study on second-order slip flow models in channels of various cross sections. *Heat Transf. Eng.* 39(11): 933–945

[46] Abramowitz M and Stegun I A 1972 Handbook of Mathematical Functions. Dover Publications, New York

[47] Cetin B and Bayer O 2011 Evaluation of Nusselt number for a flow in a microtube using second-order slip model. *Therm. Sci.* 15(suppl. 1): 103–109

[48] Su L, Duan Z, He B, Ma H, Ning X, Ding G and Cao Y 2020 Heat transfer characteristics of thermally developing flow in rectangular microchannels with constant wall temperature. *Int. J. Therm. Sci.* 155: 106412

[49] Colin S 2012 Gas microflows in the slip flow regime: A critical review on convective heat transfer. *J. Heat Transf.* 134(2)